Melting and Freezing of Metal Clusters

Andrés Aguado[1] and Martin F. Jarrold[2]

[1]Departamento de Física Teórica, Universidad de Valladolid, Valladolid 47011, Spain

[2]Chemistry Department, Indiana University, Bloomington, Indiana 47401;
email: aguado@metodos.fam.cie.uva.es, mfj@indiana.edu

Annu. Rev. Phys. Chem. 2011. 62:151–72

First published online as a Review in Advance on December 3, 2010

The *Annual Review of Physical Chemistry* is online at physchem.annualreviews.org

This article's doi:
10.1146/annurev-physchem-032210-103454

0066-426X/11/0505-0151$20.00

Keywords

thermodynamics, heat capacity, latent heat

Abstract

Recent developments allow heat capacities to be measured for size-selected clusters isolated in the gas phase. For clusters with tens to hundreds of atoms, the heat capacities determined as a function of temperature usually have a single peak attributed to a melting transition. The melting temperatures and latent heats show large size-dependent fluctuations. In some cases, the melting temperatures change by hundreds of degrees with the addition of a single atom. Theory has played a critical role in understanding the origin of the size-dependent fluctuations, and in understanding the properties of the liquid-like and solid-like states. In some cases, the heat capacities have extra features (an additional peak or a dip) that reveal a more complex behavior than simple melting. In this article we provide a description of the methods used to measure the heat capacities and provide an overview of the experimental and theoretical results obtained for sodium and aluminum clusters.

INTRODUCTION

Dynamic phase coexistence: a situation in which the system fluctuates between being entirely liquid or entirely solid at the melting/freezing transition; this behavior is found in small systems

Static phase coexistence: a situation in which the two phases coexist in contact at the melting/freezing transition; this behavior is found in large systems

Geometric shell: for a structure for which the atoms are organized in layers, particularly stable clusters can emerge when a layer is finished; e.g., for icosahedral packing there are geometric shell closings at 55 and 147 atoms

The melting of a macroscopic crystal is a first-order phase transition. At a given external pressure, the crystal melts at a single temperature at which there is a spike in the heat capacity due to the latent heat. The reverse process, freezing, often occurs at a temperature significantly below the thermodynamic melting temperature (T_m) because freezing is a nucleated process and the rate of critical nucleus formation increases as the temperature is lowered. Melting is usually not nucleated (i.e., crystals melt at $T = T_m$) because many surfaces premelt, i.e., acquire a thin liquid layer, a few atomic layers thick, as T_m is approached (1–3).

If we reduce the size of a macroscopic object, there is initially no noticeable effect on the melting temperature. The rate of critical nucleus formation is proportional to the volume, so the liquid becomes more deeply supercooled before it freezes. The supercooling of metal droplets with micrometer diameters was studied by Turnbull and collaborators (4–6) in the early 1950s.

If the size is decreased into the nanometer regime, the surface-to-volume ratio increases so that the surface energy begins to make an important contribution to the overall energy. Pawlow (7, 8) recognized in 1909 that this leads to a depression of the melting point (because the liquid has a lower surface energy than the solid) and predicted that the depression should show a $1/r$ dependency. The melting point depression has been confirmed for many metals (9–13). In the case of gold (bulk melting point 1,337 K), 3.8-nm diameter particles (approximately 1,700 atoms) melt at ~1,000 K, and 2.5-nm particles (approximately 500 atoms) melt at ~500 K (11). If this behavior continues, small gold clusters will be liquid at room temperature.

The melting point depression described above results from thermodynamic scaling of the surface and bulk contributions to the total energy, and the depression is expected to scale smoothly with particle size. For large particles this is undoubtedly true. But if we continue to decrease the particle size, at some point its properties must start to show size-dependent fluctuations. In this size regime, adding a single atom could have a dramatic effect on the melting temperature.

The melting points for large particles mentioned above were obtained by monitoring diffraction patterns of individual supported particles as a function of temperature. This approach runs into several problems for small particles or clusters. First, the substrate may perturb the properties, and second (as we expect size-dependent fluctuations) we need an approach that enables measurements for clusters with a known number of atoms. It is only recently that methods have been developed that allow melting temperatures to be determined for unsupported, single-sized metal clusters as a function of the number of atoms.

Although the small size regime has been a challenge to study experimentally, it has been a prolific area for theoretical studies (14–29). The earlier theoretical studies employed empirical potentials, but nevertheless they provided many fascinating predictions, such as that small clusters display a dynamic phase coexistence, instead of the static phase coexistence of macroscopic objects (22, 27, 28).

The first attempt to examine the melting of unsupported metal clusters was by Martin et al. (30). Their method is based on the disappearance of geometric shell structure in the mass spectra of clusters as they are heated. However, it does not provide information for single-sized clusters. It was the work of Haberland and collaborators (31, 32) that provided the real breakthrough. The main challenge with studying melting transitions for unsupported clusters is determining when they melt. Two basic approaches have been used. The most widely used methods hinge on measuring heat capacities as a function of temperature. The melting temperature is determined from the peak in the heat capacity due to the latent heat. In the other method, ion mobility measurements (33) are used to detect the shape or volume change associated with the melting transition. Experimental studies have now been performed for a variety of cluster materials including sodium (31, 32, 34–41),

tin (42–44), gallium (45–47), aluminum (48–56), sodium chloride (57), mixed metal clusters [Ga_nAl (58), Al_nCu (59)], sodium clusters doped with an oxygen atom (Na_nO) (60), and water (61). These measurements have stimulated a number of theoretical studies (49, 62–67). By far the most extensive body of work has been performed for sodium and aluminum clusters, and many features of the melting of these clusters are now understood thanks to a series of careful theoretical studies. In this article we focus on sodium and aluminum.

Whereas the melting points of large particles are always depressed, this behavior does not always continue into the small size regime. Small tin and gallium clusters, for example, have melting temperatures considerably above the bulk value (42, 44, 45). This behavior has been attributed to the clusters having different bonding than the bulk (68–71).

EXPERIMENTAL METHODS

Most of the methods used to measure melting temperatures of unsupported clusters are based on measuring the heat capacity as a function of temperature. Calorimetry measurements for macroscopic systems are performed by measuring the temperature as a function of the added energy. This approach does not work for unsupported clusters: Although their initial temperature can be fixed, there is no way to measure it after a known amount of energy has been added. The three methods described here use dissociation to define a reference state that is used to determine the internal energy change associated with a temperature change (31, 40, 45). They all start with the preparation of thermalized, size-selected clusters. The need to generate size-selected clusters calls forth mass spectrometry, which in turn means that the measurements must be performed on ions rather than neutral clusters, although both anions and cations can be studied.

The cluster ions are thermalized by passing them through a temperature-regulated region containing a buffer gas. Collisions with the buffer gas bring the clusters to the temperature of the walls. Once thermalized, they are in a canonical ensemble. They are then removed to a high-vacuum environment, where they are mass selected and then probed to determine their internal energy content. In high vacuum, the collision rate is too slow, and the rates of emission and absorption of radiation are too small, to perturb significantly the internal energy distribution before the measurement is completed.

In the method of Haberland and collaborators (31), the size-selected cluster ions are irradiated with a laser, undergo multiphoton absorption, and subsequently dissociate. This approach has been applied mainly to study sodium clusters. The dissociation energies of the sodium clusters are around 1 eV (72), three to four times smaller than the photon energy. In the multiphoton absorption step, enough energy is absorbed to reach the dissociation threshold, and then every additional photon leads to the loss of an extra three to four sodium atoms. Thus the fragment ion mass spectrum shows oscillations with peaks separated by three to four atoms. If more energy is added to the dissociating clusters, either by raising their initial temperature or by changing the photon energy, the peaks in the fragment mass spectrum shift toward smaller product ions. The heat capacity is deduced by tracking the shift in the fragment mass spectrum as the initial temperature is changed. A drawback of this approach is that the photon energy needs to be much larger than the cluster dissociation energy (which so far has limited this method to weakly bound clusters).

The method of Jarrold and collaborators (45, 73) uses multicollision-induced dissociation. The cluster ions are directed into a collision cell containing helium, and the initial kinetic energy required to dissociate 50% of the clusters (KE50%D) is determined. Then the temperature is changed and KE50%D is measured again. The heat capacity is proportional to the change in KE50%D divided by the change in temperature. The proportionality constant is the fraction of the cluster ions' kinetic energy that is converted into internal energy (74, 75) by collisions with

the helium. This is determined from an impulsive collision model. This approach can be applied to all clusters (strongly bound and weakly adsorbing). The main drawback is that the energies are not referenced directly to an absolute scale.

In the method of L'Hermite and collaborators (40), the internal energy is probed by determining how many atoms will stick to the clusters. It has been used to investigate the melting of sodium clusters. Size-selected cluster ions at a well-characterized temperature are passed through a collision cell containing sodium vapor, where additional sodium atoms stick:

$$Na_n^+ + mNa \rightarrow Na_{n+m}^+.$$

Every time a sodium atom sticks to the cluster, the internal energy increases by the dissociation energy plus the collision energy. As more atoms stick, the internal energy increases to the point at which evaporation limits further cluster growth. A cold cluster can accommodate more atoms before reaching the evaporative limit than a hot one. Heat capacities are deduced from measurements of the number of sodium atoms that stick as a function of temperature and kinetic energy.

Global minimum (GM): the lowest energy structure that exists on the ground state of the potential energy hypersurface

MD: molecular dynamics

DFT: density functional theory

OF-DFT: orbital-free density functional theory

THEORETICAL METHODS

A theoretical analysis of cluster melting transitions requires a simulation model and a method to calculate the cluster energy. The simulation model has to provide information about both solid and liquid phases. At zero Kelvin, and dispensing with nuclear quantum effects, the cluster adopts a single solid structure that minimizes the cluster potential energy. Locating this global minimum (GM) structure is a complex optimization problem for which a variety of algorithms, such as genetic (76) or basin hopping (77), have been developed and reviewed (78). The melting transition usually is studied by modeling the heating of the GM structure, either with molecular dynamics (MD) or Monte Carlo techniques (79). MD generates the true dynamics of the cluster and thus provides access to kinetic effects and dynamical properties like time-correlation functions. Monte Carlo is a stochastic method that efficiently samples the appropriate statistical ensemble and provides faster access to static properties. Both methods suffer from potential broken ergodicity (incomplete sampling) problems (80), which may be alleviated by using multiple histogram (81) or parallel tempering (82) methods, for example. Path-integral techniques (83) can be employed if quantum nuclear effects are important (as in water clusters).

The most accurate cluster energies are provided by ab initio quantum chemistry methods (84), which are limited to very small clusters due to their unfavorable scaling with size. A reliable MD simulation of cluster melting has to be at least several nanoseconds long, so quantum chemistry methods typically are not employed. Methods based on density functional theory (DFT) (85) provide a good compromise between accuracy and efficiency, mostly when coupled with pseudopotentials (86) to describe the most internal electrons. They are the methods of choice to study the melting transition of clusters with approximately 100 atoms. Other methods like tight-binding (87) or orbital-free (OF-)DFT (88) can handle up to several thousand atoms and still include an explicit (although approximate) description of the electronic density. Finally, empirical potentials are most efficient by dispensing completely with the quantum nature of the problem. If properly parameterized, they can provide useful semiquantitative information for clusters with more than 1,000 atoms or for the more complex case of nanoalloys (89, 90).

MELTING-LIKE TRANSITION IN SODIUM CLUSTERS

Figure 1 shows typical examples of canonical caloric curves for sodium clusters. The melting transition is broadened by finite size effects and covers a finite-temperature interval. The derivative

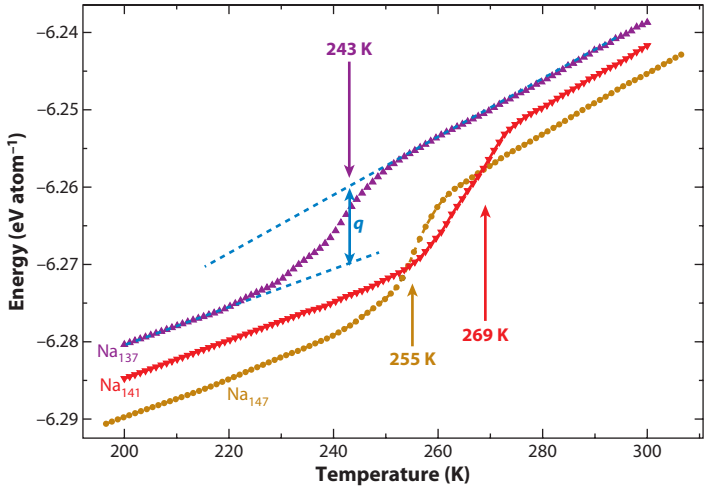

Figure 1

Three representative examples of caloric curves for sodium clusters obtained from orbital-free density functional theory simulations. Note the nonmonotonic size dependence of the melting temperatures (*arrows*). Figure adapted with permission from Reference 110. Copyright (2005) by the American Chemical Society.

of the caloric curve is the canonical heat capacity. The location of the peak in the heat capacity (or the maximum slope in the caloric curve) is usually taken to be the melting temperature, T_m. The energy shift between the solid and liquid branches of the caloric curve (which is equal to the area under the heat capacity peak) determines the latent heat, q_m. The entropy change for melting, ΔS_m, then can be determined from $T_m = q_m/\Delta S_m$.

A summary of the measured T_m values is offered in **Figure 2**. The calorimetric measurements of Haberland and collaborators (Freiburg group) for Na_n^+ clusters with $n = 55$–360 atoms show a markedly nonmonotonic dependency of T_m with cluster size (32, 37, 39). Maxima in T_m do not correlate with electronic shell closings (which dominate most other properties of sodium clusters) (91) or with geometrical shell closings for icosahedral packing. T_m values are depressed by almost 40% with respect to the bulk, and moreover the average trend is for T_m to decrease with increasing size. For clusters with 1,000–10,000 atoms [measurements by Martin and collaborators (30)], T_m is still depressed by 20%, and a clear extrapolation to the bulk value is still not visible.

The measured q_m and ΔS_m values also show a nonmonotonic size dependence. However, most local maxima in q_m and ΔS_m correlate with known icosahedral shell closings. This observation led Haberland et al. (39) to conclude that q_m and ΔS_m yield more useful information than their ratio T_m and that the size dependence of the melting of sodium clusters is determined mostly by geometrical effects. The strong correlation between q_m and ΔS_m suggests that the more stable clusters also have stiffer bonds and a more-perfect structural order.

Early computer simulations of the melting-like transition (25, 26, 92–100) achieved only partial success at reproducing and interpreting the measurements for sodium clusters: In particular, the detailed size oscillations in the melting properties were not reproduced, and many of the simulated heat capacities showed strong premelting peaks, in marked disagreement with experiment. This led Calvo & Spiegelmann (101) to conclude that empirical potentials are qualitatively inadequate for this problem. Manninen and coworkers (102–105) reported MD simulations at the DFT level. Although the simulations were so short that thermal equilibrium was not well established, they reproduced the experimental observation that $T_m(Na_{55}^+) > T_m(Na_{93}^+)$. Similar results were obtained in longer MD simulations by Chacko et al. (106).

Electronic shell: the valence electrons in metal clusters are arranged in electronic shells due to angular momentum restrictions (like the electrons in an atom); particularly stable clusters occur at electronic shell closings

Premelting: a peak or a shoulder in the heat capacity at a lower temperature than the melting transition

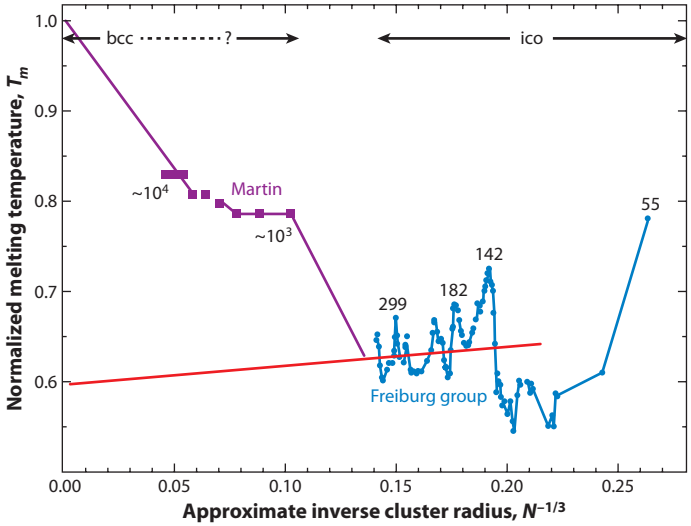

Figure 2

Melting temperatures measured for sodium clusters as a function of the inverse cluster radius. The T_m values are shown normalized to the bulk limit. The results of Haberland and collaborators (Freiburg group) (32, 37, 39) for clusters with 55–360 atoms are shown together with those of Martin and coworkers (30) for clusters with 10^3–10^4 atoms. The red line is a linear regression to the Freiburg group results. For small sizes the clusters are based on icosahedral packing (ico). At some (unknown) critical size, there must be a transition toward bulk-like (bcc) structures.

Aguado & López (107) reproduced the oscillations in the measured T_m over a broad size range (n = 55–299; see **Figure 3**) using OF-DFT MD simulations. Clusters with higher T_m values were found to be more compact and to have a higher surface stability. Noya et al. (108) reported the putative GM structures of Na_n clusters with up to 380 atoms, obtained with a Murrell-Mottram empirical potential (see **Figure 4**). The accuracy of this potential was supported by reoptimizations at the OF-DFT level and later confirmed by photoelectron spectroscopy (109) for many sizes [although Ghazi et al. (67) have reported different DFT GM structures for clusters with approximately 92 atoms]. The theoretical magic numbers (enhanced cohesive energies) showed excellent agreement with the local maxima in the measured latent heats. For sizes intermediate between two icosahedral shell closings, the GM structures undergo unusual twisting distortions, which generate a more stable surface, consisting entirely of {111}-like facets.

The detailed size dependency of melting properties over a narrow size range, n = 135–147, also has been reproduced in DFT simulations (41, 52, 110). Here the cohesive energy has a local maximum at the icosahedral shell closing (n = 147 atoms), and a large drop at n = 148. Moreover, the cohesive energy of a solid-like cluster with 138 electrons (an electronic shell closing) is not enhanced significantly. The cohesive energies, which correlate with the experimental latent heats (see below), thus are determined mostly by geometric effects for clusters of this size (52). The entropy of melting also has a local maximum at n = 147. The reduction in ΔS_m for smaller sizes has been interpreted in terms of a premelting mechanism involving the diffusive motion of atomic vacancies at the surface (41, 110), in agreement with a combinatorial entropy model advanced by Haberland et al. (39).

Although electronic shell effects are of minor importance for the melting of large sodium clusters, simulations suggest this is not true for small clusters (111, 112). Here the electron density is confined to a smaller volume, and the addition or removal of a single electron can induce a

Magic number: a particularly stable cluster size; stability could result from an electronic shell closing, a geometric shell closing, or both

Cohesive energy: the total binding energy (atomization energy) of a cluster divided by the number of atoms

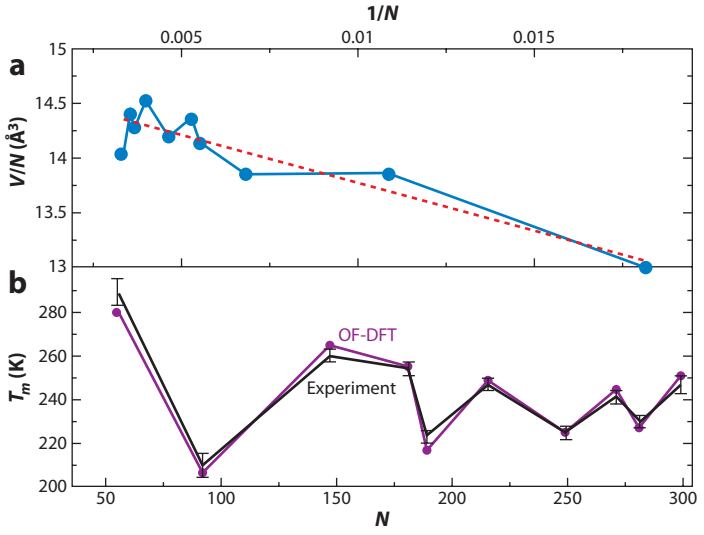

Figure 3

(*a*) Average volume per atom as a function of size. The red dashed line is a linear regression to the data. (*b*) The melting points determined through orbital-free density functional theory (OF-DFT) molecular dynamics simulations. The simulations reproduce the experimentally observed oscillations in the size range $n = 55$–299. Clusters that are more compact melt at a higher temperature. Figure adapted with permission from Reference 107. Copyright (2005) by the American Physical Society.

significant change in the cohesive energies. For example, Ghazi et al. (111) predicted that $T_m(Na_{39}^-)$ is 40 K higher than $T_m(Na_{39})$ due to the electron shell closing at 40 electrons. These jellium-like effects also induce significant shape deformations in both solid and liquid clusters (102–105).

The width of the heat capacity peak generally decreases with increasing cluster size, approaching the bulk limit of an infinitely narrow transition. Small clusters, in contrast, melt gradually over a broad temperature interval. The measured specific heat of Na_{41}^+ evolves continuously from a solid value of $3.3k_B$ to a liquid value of approximately $4.1k_B$ (38). The temperature dependency

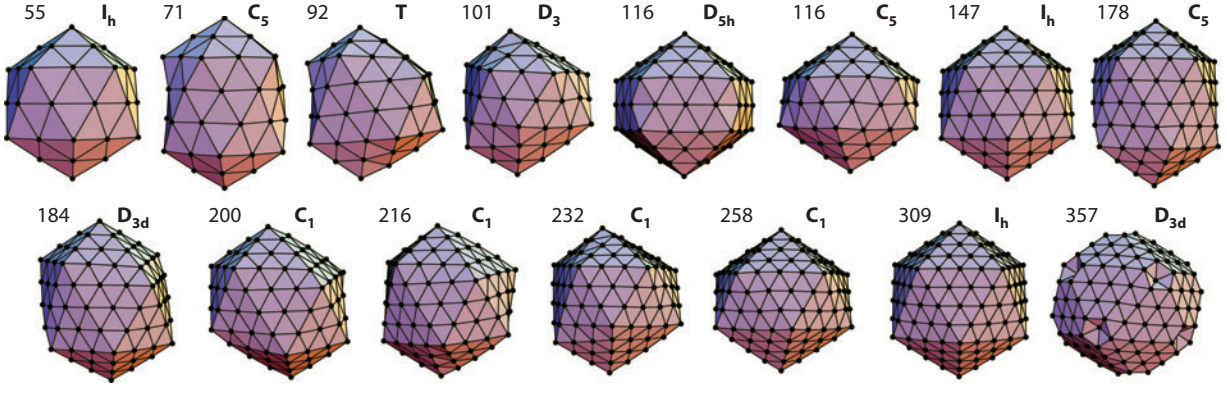

Figure 4

A selection of sodium cluster global-minimum structures that have enhanced stabilities. The structures are labeled by their size and point group symmetry. Figure adapted from Reference 108 with kind permission of the *European Physical Journal*.

Postmelting: a peak or a shoulder in the heat capacity at a higher temperature than the melting transition

Surface layering: in an otherwise disordered liquid, the atoms or molecules in the near-surface region are stratified into well-defined layers parallel to the surface; the layering decays rapidly away from the surface

of the photoabsorption spectrum (113, 114) also suggests a gradual melting process: Cold clusters show electronic transitions between discrete molecular orbital levels, whereas for hot liquid clusters the spectrum agrees with a jellium model of confined electrons in a spheroidal well. The simulations (115–117) reveal how the liquid phase is approached gradually through isomerizations between different cluster structures, which start at temperatures as low as 30 K and involve the cooperative movement of all the atoms in the cluster. The barriers against these cooperative atomic displacements are expected to scale extensively with size, so this mechanism is relevant only for sufficiently small clusters. Some large clusters also may show a broad transition with a small latent heat, if the structure of the solid cluster is amorphous (118). In some cases, such as Na_{59}^+, the amorphous GM structure may be driven by an electronic shell closing, which forces the atoms to adopt a spherical shape (104).

The cluster heat capacities also can show postmelting features, i.e., small peaks or shoulders at $T > T_m$. For example, the caloric curve of Na_{147}^+ shows such a feature at 40 K above T_m (41). This postmelting feature has been attributed to the presence of surface layering in the liquid cluster (see **Figure 5**), a property shared by extended liquid metal surfaces. The surface layering is size dependent. For Na_{147}^+, which has a nonmelting surface (41), the layering is sufficiently strong to effectively confine the 13 innermost atoms in a solid-like phase even above T_m; the cluster core cannot melt completely until 40 K above T_m. Na_{139}^+, in contrast, has some atomic vacancies at the surface, which facilitates radial atomic diffusion; the layering is correspondingly not so strong and no postmelting anomaly is observed. Postmelting anomalies have been observed in simulations of very small clusters such as Na_{25} (119). In this case they are the cluster analog of a liquid-liquid phase transition between two liquid phases with different average densities.

There is an interesting theoretical prediction concerning the melting-like transition in clusters and the nonequivalence of statistical ensembles for finite, nonextensive systems. In the

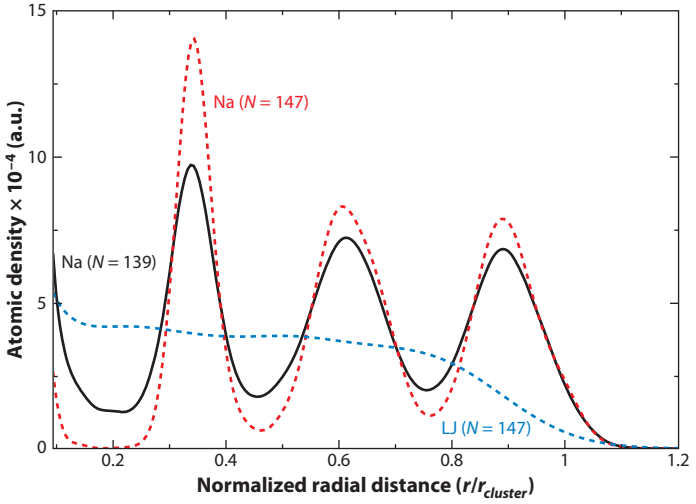

Figure 5

Calculated radial atomic densities of Na_{147} and Na_{139} as a function of normalized distance, where $r_{cluster}$ is the cluster radius and r measures the distance from the cluster's center of mass. The results correspond to a temperature that is above T_m but below the postmelting temperature; i.e., the core of Na_{147} is still solid. The layering has a larger amplitude for Na_{147}: The first minimum even touches the r axis, demonstrating that the central atom does not diffuse at this temperature, a clear indicator of postmelting. A 147-atom Lennard-Jones (LJ) cluster just above T_m (*blue dashed line*), conversely, shows no layering at all. Figure adapted with permission from Reference 41. Copyright (2009) by the American Physical Society.

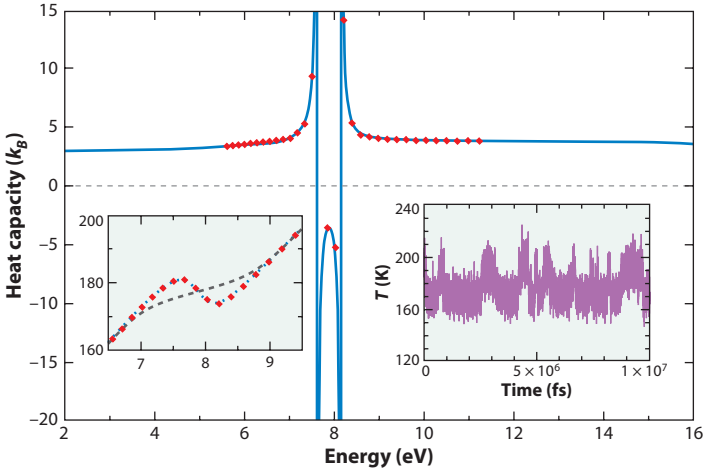

Figure 6

Microcanonical heat capacity of Na_{147} obtained from parallel tempering Monte Carlo simulations (122). The lower-left inset shows the microcanonical and canonical (*gray dashed line*) caloric curves. The lower-right inset shows the time evolution of the kinetic temperature at an energy within the dynamical coexistence range. Figure adapted with permission from Reference 122. Copyright (2008) by the Europhysics Letters Association.

microcanonical ensemble, the basic quantity (from which all the thermodynamic information may be extracted) is the entropy, $S = k_B \ln \Omega$. In finite systems S is a nonextensive quantity and may develop a dent with an inverted curvature for energies within the dynamical coexistence range. If this is the case, the microcanonical caloric curve acquires a negative slope (or undergoes backbending) and the heat capacity becomes negative at melting. The canonical energy distribution becomes bimodal, with a deep minimum between the peaks corresponding to solid and liquid phases. The S dent implies a reduced number of states at the melting energies: States with solid and liquid phases in contact (static coexistence) are shifted to higher energies because of the interfacial free energy (which is not negligible in a finite system), and dynamical coexistence occurs instead. The latent heat must be larger than typical excitation energies under coexistence conditions in order to observe a negative heat capacity (120). A negative heat capacity has been inferred for Na_{147}^+ from the experiments by Schmidt et al. (35), and it has been reproduced in simulations (121, 122) (see **Figure 6**). Michaelian and coworkers (123) have argued that the negative heat capacity is an artifact due to broken ergodicity (trapping in a restricted region of phase space). However, there is sufficient evidence and quite a general consensus (122, 124) that the S dent is a real feature of nonextensive systems.

MELTING-LIKE TRANSITION IN ALUMINUM CLUSTERS

Heat capacities have been measured for aluminum cluster cations (16–128 atoms) and anions (35, 70) using multicollision-induced dissociation. **Figure 7** shows heat capacities recorded for aluminum cluster cations with 40, 42, 43, and 37 atoms (50). All clusters in **Figure 7** show a single peak, which is attributed to a melting transition. As noted above, the melting of small clusters is thought to involve a dynamic coexistence between the solid-like and liquid-like states, in which the entire cluster fluctuates between solid and liquid. Dynamic phase coexistence can be treated as a two-state transition (equilibrium) between the solid-like and liquid-like states (125). This leads

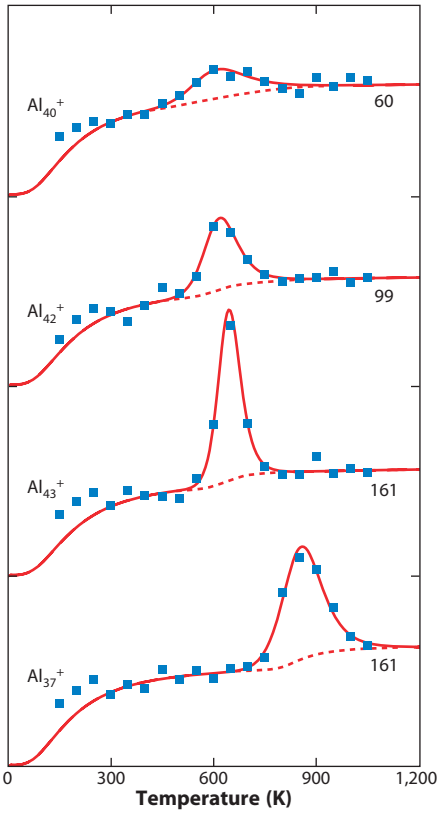

Figure 7

Plot of the heat capacities for aluminum cluster cations with 40, 42, 43, and 37 atoms (50). The blue squares show the measured heat capacities, and the red lines show fits using a two-state melting model that invokes an equilibrium between solid-like and liquid-like clusters. The numbers on the right-hand side of the figure show the latent heat associated with each melting transition in kilojoules per mole. Al_{40}^+, Al_{42}^+, and Al_{43}^+ have approximately the same melting temperatures while the latent heat increases with the cluster size. The melting transition becomes narrower as the latent heat increases, as expected for a two-state transition. Al_{37}^+ has the same latent heat as Al_{43}^+, but it melts at a significantly higher temperature. The transition for Al_{37}^+ is broader than for Al_{43}^+, in agreement with the prediction of the two-state model.

to a straightforward prediction for the width and height of the peak in the heat capacity (**Figure 7**) and its dependency on the latent heat and T_m. The peaks get broader as the latent heat decreases and as T_m increases because the solid-like and liquid-like states coexist over a broader temperature range.

The heat capacities of some clusters show two peaks. Results for Al_{115}^+ are illustrated in **Figure 8**. Similar behavior was found for Al_{116}^+ and Al_{117}^+ (54). These are the only clusters for which two clearly resolved peaks were observed. For some other clusters, the heat capacity peak is bimodal or broadened, indicating that melting does not occur through a simple two-state transition.

There are many examples in which two heat capacity peaks have been observed in simulations (71, 95, 97, 101, 117, 118, 126–128). This behavior is usually called premelting when the low-temperature peak is the smaller of the two and postmelting for the reverse situation. However, multiple peaks are rare in experimental studies. As noted above, a high-temperature shoulder on

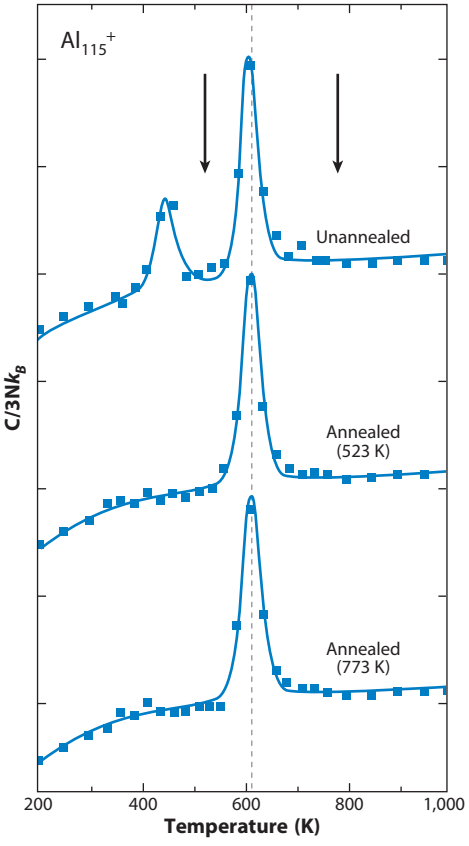

Figure 8

Heat capacities recorded for Al_{115}^+. The upper plot shows results for unannealed Al_{115}^+. The middle plot is for an annealing temperature of 523 K (between the two peaks in the upper plot). The lower plot is for an annealing temperature of 773 K (above both peaks). The arrows on the upper plot show the two annealing temperatures. Figure adapted with permission from Reference 54. Copyright (2009) by the American Physical Society.

the heat capacity peak for Na_{147}^+ is attributed to liquid layering (41). For aluminum, there are several examples of both premelting (Al_{51}^+, Al_{52}^+, Al_{115}^+, Al_{116}^+, and Al_{117}^+) (48, 51, 54) and postmelting (Al_{61}^+ and Al_{83}^+) (50, 51).

Excluding electronic effects, there are three main causes for a second feature in the heat capacity plot: (*a*) partial melting, in which the surface or some other part of the cluster melts at a lower temperature than the rest; (*b*) two structural isomers that melt at different temperatures; and (*c*) a solid-to-solid transition followed by melting.

Structural transitions have been seen to precede melting in a number of recent simulations (129–136). For example, in simulations of palladium clusters, transitions from both fcc and decahedral ground states to icosahedral structures precede melting (136). Solid-solid structural transitions are frequently found to precede melting for Lennard-Jones clusters, resulting in two well-resolved peaks in the heat capacity (137–143).

Annealing studies were performed for Al_{115}^+, Al_{116}^+, and Al_{117}^+ to shed light on the origin of the two peaks (54). In these experiments the clusters were heated and held at an elevated temperature before having their temperature set for the heat capacity measurements. Al_{115}^+ was annealed to

523 K and 773 K (see arrows in **Figure 8**). In both cases the low-temperature peak disappeared and the high-temperature peak was unaffected. Based on these results, the low-temperature peak is attributed to a structural transition (54) and the high-temperature peak to the melting of the higher-enthalpy structure generated in the structural transition. The structural transition involves a superheated solid (it does not occur under equilibrium conditions).

A peak in the heat capacity indicates a transition to a higher enthalpy, but entropically preferred state. For some clusters with approximately 60 and 80 atoms, there is a dip in the heat capacities at a slightly lower temperature than the peak (51). A dip in the heat capacity indicates a transition to a lower enthalpy state. For example, a dip could result from a structural transition from a poorly formed (amorphous) geometry generated during cluster growth to a lower-energy structure. If this explanation is correct, the dips should disappear when the clusters are annealed, but for many clusters the dips persist. The behavior of the dips can be reproduced using a simple kinetic model of melting and freezing in a system of one liquid-like and two solid-like states with different melting temperatures and latent heats. The dips result from freezing into a high-energy geometry and then annealing into the thermodynamically preferred solid. The thermodynamically preferred solid has the higher freezing temperature. However, the liquid can bypass freezing into the thermodynamically preferred solid (at high cooling rates) if the higher-energy geometry has a larger freezing rate (just like glass formation in the macroscopic world).

Figure 9 shows melting temperatures and latent heats from Al_{25}^+ (the smallest cluster to show a heat capacity peak) to Al_{128}^+. Most clusters have melting temperatures below the bulk value,

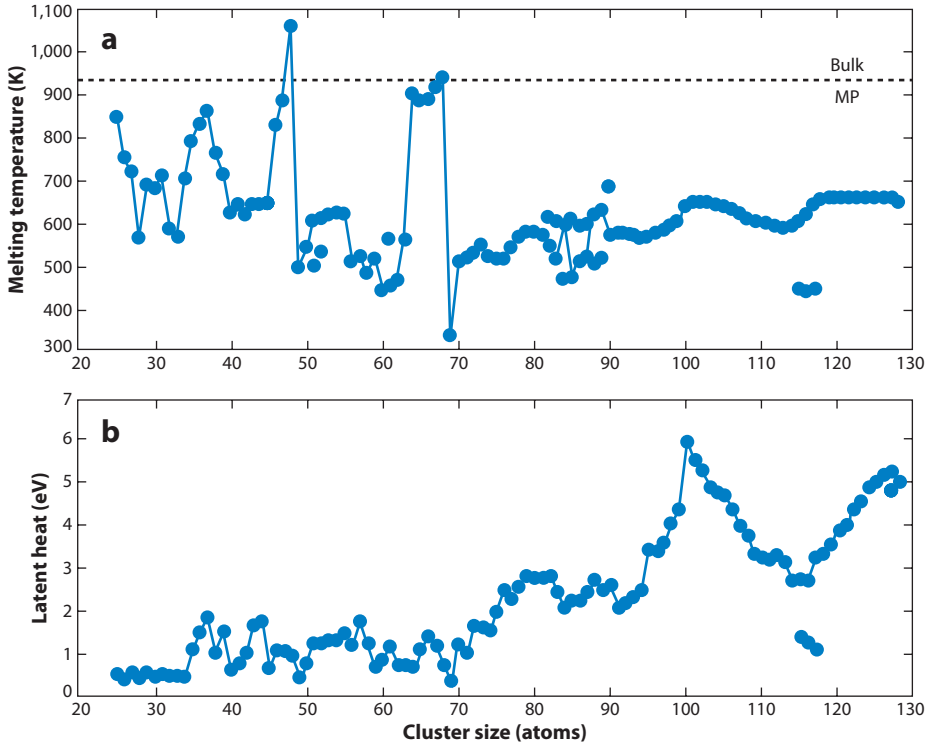

Figure 9

Melting temperatures (*a*) and latent heats (*b*) for aluminum cluster cations with 25 to 128 atoms.

but the melting temperatures do not drop systematically with decreasing cluster size. There are large fluctuations in the melting temperatures for clusters with less than 90 atoms, and smoother oscillations for $n > 90$. The latent heats also show large fluctuations that are not correlated with the melting temperatures. Efforts to understand the fluctuations in melting temperatures and latent heats using empirical potentials have been largely unsuccessful (62–64).

Fluctuations in the latent heats are correlated with fluctuations in the cohesive energies of solid clusters (52). Usually, dissociation energies for metal clusters are measured by adding energy until

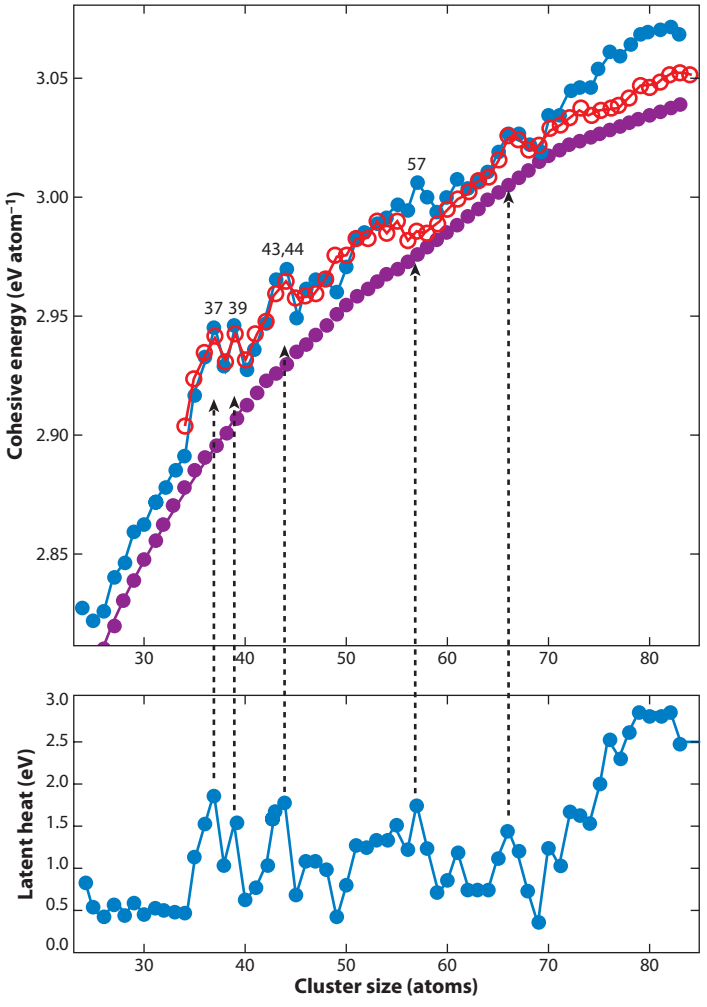

Figure 10

Plots showing the correlation between the latent heats and the cohesive energies of solid clusters (52). The purple solid circles represent the cohesive energies of liquid clusters. The blue solid circles represent the cohesive energies of solid clusters (which are determined from the cohesive energies of liquid clusters and the latent heats). The red open circles show cohesive energies for the lowest energy structures found in an extensive geometry search with density functional theory. The measured and calculated cohesive energies are in good agreement except for a few clusters around Al_{57}^+ and for clusters larger than 71 atoms. For these clusters, the calculated cohesive energy is smaller than the measured value, and it is likely that the lowest energy structure has not been found in the calculations.

the cluster dissociates (72, 144–147). For clusters with more than a few atoms, an excess energy (i.e., beyond the dissociation energy) is required for dissociation to occur on the experimental timescale. Then, the dissociation energy is deduced using a statistical model to account for the excess energy. For clusters that melt, this procedure provides the dissociation energy for the liquid cluster, because dissociation occurs from the liquid state. **Figure 10** shows cohesive energies determined using this sort of approach for liquid aluminum cluster cations (52). As expected, the cohesive energies of the liquid clusters change smoothly with cluster size, suggesting that electron shell closing effects are not significant in liquid aluminum clusters. The cohesive energies of the solid clusters are given by

$$C_S(n) \approx \frac{L(n) + C_L(n)}{n},$$

where $C_L(n)$ is the cohesive energy of the n atom liquid cluster, and $L(n)$ is the latent heat. As $C_L(n)$ does not show significant size-dependent fluctuations, fluctuations in the cohesive energies of the solid-like clusters result almost entirely from fluctuations in the latent heats (52).

Measured cohesive energies for the solid clusters also are shown in **Figure 10**. There are significant fluctuations in the cohesive energies of the solid clusters. **Figure 10** additionally shows cohesive energies for the lowest energy structures found using an extensive search with DFT. Four groups of low-energy structures were found: distorted decahedral fragments, fcc fragments, fcc fragments with stacking faults, and disordered structures (see **Figure 11** for examples) (52). The

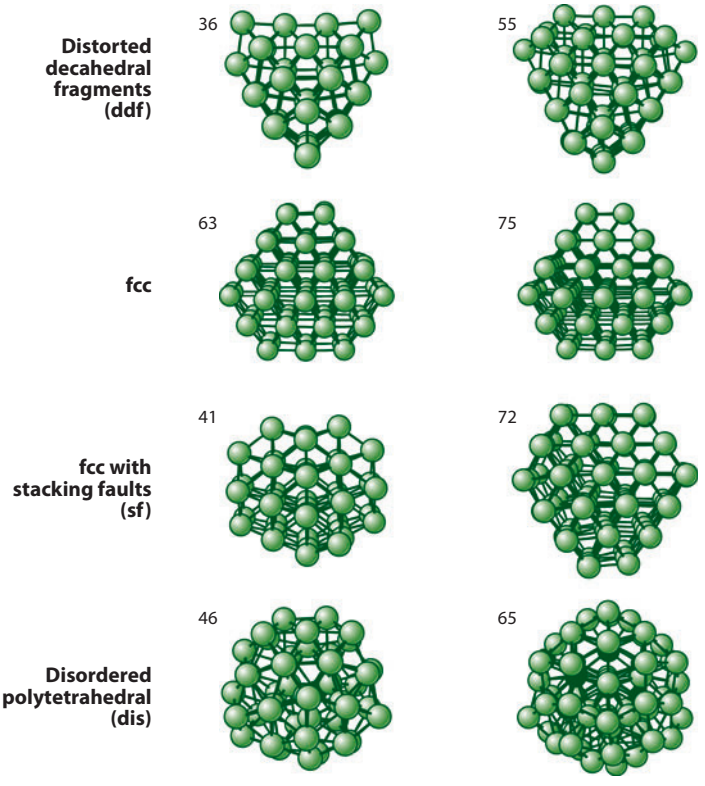

Figure 11

Examples of the four types of geometry found for aluminum clusters in the density functional theory calculations.

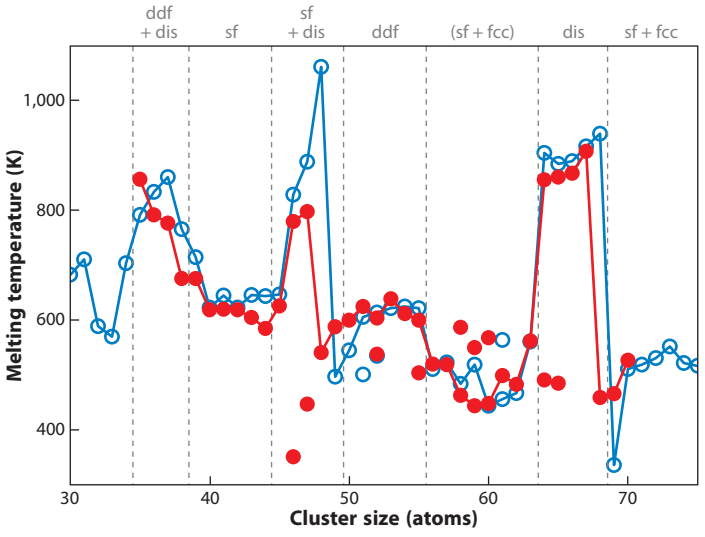

Figure 12

Comparison of the melting temperatures for aluminum cluster cations (*blue open circles*) and anions (*red solid circles*). The gray notations along the top of the plot identify the lowest energy structure from DFT calculations associated with each size range: ddf, distorted decahedral fragments; fcc, fcc fragments; sf, fcc fragments with stacking faults; and dis, disordered structures. Large changes in the melting temperatures are correlated with structural changes. Figure adapted with permission from Reference 55. Copyright (2009) by the American Physical Society.

measured and calculated cohesive energies (**Figure 10**) are correlated strongly for most cluster sizes. According to the calculations, the variations in the cohesive energies (and the latent heats) result from a combination of geometric and electronic shell effects. For some clusters an electronic shell closing is responsible for the enhanced cohesive energy and latent heat (e.g., $n = 37$), whereas for others (e.g., $n = 44$) a structural shell closing is the cause.

Figure 12 compares melting temperatures determined for aluminum cluster anions and cations (55). The melting temperatures for the anions and cations show the same general features, but those for the anions are shifted to slightly smaller sizes. The large variations in the melting temperatures are correlated with changes in the structure of the clusters. For example, the maximum in the melting temperatures around 66 atoms is associated with the clusters adopting disordered geometries that result from a spherical electronic shell closing with 198 valence electrons. The electronic shell closing forces the cluster to adopt a near-spherical geometry, which has much less local order than the other geometries. As a consequence, the entropy change on melting is smaller, and this causes an elevated melting temperature according to $T_m = q_m/\Delta S_m$. The downward shift in the anion features in **Figure 12** is probably an electronic effect (the anion has two more valence electrons than the cation).

FUTURE WORK

The studies described here barely scratch the surface of cluster melting and freezing, and there are many interesting and important questions that remain to be addressed. For example, it is not known at what size the liquid and solid phases of a cluster start to coexist in contact; virtually nothing is known about the kinetics of cluster melting and freezing transitions and how the rates change with size. The properties of the highly confined liquid clusters remain a largely unexplored area,

although studies of the chemical properties of liquid aluminum clusters show that large changes in reactivity can be associated with the melting transition (148, 149). The interplay between structure, dynamics, phase, and reactivity has connections to catalysis. Finally, we mention the vast and virtually unexplored area of bimetallic clusters and the potential for tailoring properties at the nanometer length scale with alloys and core-shell arrangements.

SUMMARY POINTS

1. Metal clusters with fewer than 100 atoms show melting/freezing transitions.
2. The melting temperatures and latent heats show large size-dependent fluctuations.
3. In some cases, the addition of a single atom can change the melting temperature by hundreds of degrees.
4. The size-dependent variations in the latent heats are correlated with variations in the cohesive energies.
5. The size-dependent fluctuations in the melting temperatures are related mainly to structural changes.
6. In some cases the liquid clusters show evidence for layering (in which the atoms in the liquid are organized in layers).
7. The microcanonical heat capacity can become negative on melting.

DISCLOSURE STATEMENT

The authors are not aware of any affiliations, memberships, funding, or financial holdings that might be perceived as affecting the objectivity of this review.

ACKNOWLEDGMENTS

We gratefully acknowledge the support of the Spanish "Ministerio de Ciencia e Innovación," the European Regional Development Fund, and "Junta de Castilla y León" (project numbers FIS2008-02490/FIS and GR120) and the support of the U.S. National Science Foundation under grant 0911462.

LITERATURE CITED

1. Frenken JWM, van der Veen JF. 1985. Observation of surface melting. *Phys. Rev. Lett.* 54:134–37
2. Frenken JWM, Maree PMJ, van der Veen JF. 1986. Observation of surface-initiated melting. *Phys. Rev. B* 34:7506–16
3. Tartaglino U, Zykova-Timan T, Ercolessi F, Tosatti E. 2005. Melting and nonmelting of solid surfaces and nanosystems. *Phys. Rep.* 411:291–321
4. Turnbull D, Cech RE. 1950. Microscopic observation of the solidification of small metal droplets. *J. Appl. Phys.* 21:804–10
5. Turnbull D. 1950. Formation of crystal nuclei in liquid metals. *J. Appl. Phys.* 21:1022–28
6. Turnbull D. 1952. Kinetics of solidification of supercooled liquid mercury droplets. *J. Chem. Phys.* 20:411–24
7. Pawlow P. 1909. Über die abhängigkeit des schmelzpunktes von der oberflächenenergie eines festen körpers. *Z. Phys. Chem.* 65:1–35
8. Pawlow PZ. 1909. Über die abhängigkeit des schmelzpunktes von der oberflächenenergie eines festen körpers (zusatz). *Z. Phys. Chem.* 65:545–48

9. Takagi M. 1954. Electron-diffraction study of liquid-solid transition of thin metal films. *J. Phys. Soc. Jpn.* 9:359–63
10. Peppiatt SJ. 1975. Melting of small particles. II. Bismuth. *Proc. R. Soc. Lond. Ser. A* 345:401–12
11. Buffat Ph, Borell JP. 1976. Size effect on the melting temperatures of gold particles. *Phys. Rev. A* 13:2287–98
12. Couchman PR, Jesser WA. 1977. Thermodynamic theory of size dependence of melting temperatures in metals. *Nature* 269:481–83
13. Lai SL, Guo JY, Petrova V, Ramanath G, Allen LH. 1996. Size-dependent melting properties of small tin particles: nanocalorimetric measurements. *Phys. Rev. Lett.* 77:99–102
14. Alder BJ, Hoover WG, Wainwright TE. 1963. Cooperative motion of hard disks leading to melting. *Phys. Rev. Lett.* 11:241–43
15. Briant CL, Burton JJ. 1973. Melting of a small cluster of atoms. *Nat. Phys. Sci.* 243:100–2
16. McGinty DJ. 1973. Molecular dynamics studies of the properties of small clusters of argon atoms. *J. Chem. Phys.* 58:4733–42
17. Damgaard Kristensen W, Jensen EJ, Cotterill RMJ. 1974. Thermodynamics of small clusters of atoms: a molecular dynamics simulation. *J. Chem. Phys.* 60:4161–69
18. Briant CL, Burton JJ. 1975. Molecular dynamics study of the structure and thermodynamic properties of argon microclusters. *J. Chem. Phys.* 63:2045–58
19. Etters RD, Kaelberer J. 1975. Thermodynamic properties of small aggregates of rare gas atoms. *Phys. Rev. A* 11:1068–79
20. Etters RD. Kaelberer J. 1977. On the character of the melting transition in small atomic aggregates. *J. Chem. Phys.* 66:5112–16
21. Berry RS, Jellinek J, Natanson G. 1984. Unequal freezing and melting temperatures for clusters. *Chem. Phys. Lett.* 107:227–30
22. Honeycutt JD, Anderson HC. 1987. Molecular dynamics study of melting and freezing of small Lennard-Jones clusters. *J. Phys. Chem.* 91:4950–63
23. Labastie P, Whetten RL. 1990. Statistical thermodynamics of the cluster solid-liquid transition. *Phys. Rev. Lett.* 65:1567–70
24. Wales DJ, Berry RS. 1990. Freezing, melting, spinoidals, and clusters. *J. Chem. Phys.* 92:4473–82
25. Bulgac A, Kusnezov D. 1992. Thermal properties of Na_8 microclusters. *Phys. Rev. Lett.* 68:1335–38
26. Ju N, Bulgac A. 1993. Finite-temperature properties of sodium clusters. *Phys. Rev. B* 48:2721–32
27. Rose JP, Berry RS. 1993. Freezing, melting, nonwetting, and coexistence in $(KCl)_{32}$. *J. Chem. Phys.* 98:3246–61
28. Wales DJ, Berry RS. 1994. Coexistence in finite systems. *Phys. Rev. Lett.* 73:2875–78
29. Berry RS. 1997. Melting and freezing phenomena. *Microscale Thermophys. Eng.* 1:1–18
30. Martin TP, Näher U, Schaber H, Zimmermann U. 1994. Evidence for a size-dependent melting of sodium clusters. *J. Chem. Phys.* 100:2322–24
31. Schmidt M, Kusche R, Kronmüller W, von Issendorff B, Haberland H. 1997. Experimental determination of the melting point and heat capacity for a free cluster of 139 sodium atoms. *Phys. Rev. Lett.* 79:99–102
32. Schmidt M, Kusche R, von Issendorff B, Haberland H. 1998. Irregular variations in the melting point of size-selected atomic clusters. *Nature* 393:238–40
33. Clemmer DE, Jarrold MF. 1997. Ion mobility measurements and their applications to clusters and biomolecules. *J. Mass Spectrom.* 32:577–92
34. Kusche R, Hippler T, Schmidt M, von Issendorf B, Haberland H. 1999. Melting of free sodium clusters. *Eur. Phys. J. D* 9:1–4
35. Schmidt M, Kusche R, Hippler T, Donges J, Kronmüller W, et al. 2001. Negative heat capacity for a cluster of 147 sodium atoms. *Phys. Rev. Lett.* 86:1191–94
36. Schmidt M, Hippler T, Donges J, Kronmüller W, von Issendorff B, et al. 2001. Caloric curve across the liquid-to-gas change for sodium clusters. *Phys. Rev. Lett.* 87:203402
37. Schmidt M, Haberland H. 2002. Phase transitions in clusters. *C. R. Phys.* 3:327–40
38. Schmidt M, Donges J, Hippler T, Haberland H. 2003. Influence of energy and entropy on the melting of sodium clusters. *Phys. Rev. Lett.* 90:103401

29. Provides a good overview of earlier theoretical studies of the melting and freezing of mainly rare gas clusters.

31. Reports first measurement of the melting temperature and latent heat for unsupported clusters.

32. Reports the first observation of size-dependent variations in the melting temperatures of atomic clusters.

35. Reports the first experimental evidence for a negative microcanonical heat capacity.

39. Haberland H, Hippler T, Donges J, Kostko O, Schmidt M, von Issendorff B. 2005. Melting of sodium clusters: Where do the magic numbers come from? *Phys. Rev. Lett.* 94:035701
40. Chirot F, Feiden P, Zamith S, Labastie P, L'Hermite JM. 2008. A novel experimental method for the measurement of the caloric curves of clusters. *J. Chem. Phys.* 129:164514
41. Hock C, Bartels C, Straßburg S, Schmidt M, Haberland H, et al. 2009. Premelting and post-melting in clusters. *Phys. Rev. Lett.* 102:043401
42. Shvartsburg AA, Jarrold MF. 2000. Solid clusters above the bulk melting point. *Phys. Rev. Lett.* 85:2530–32
43. Bachels T, Güntherodt H-J, Schäfer R. 2000. Melting of isolated tin nanoparticles. *Phys. Rev. Lett.* 85:1250–53
44. Breaux GA, Neal CM, Cao B, Jarrold MF. 2005. Tin clusters that do not melt: calorimetry measurements up to 650 K. *Phys. Rev. B* 71:073410
45. Breaux GA, Benirschke RC, Sugai T, Kinnear BS, Jarrold MF. 2003. Hot and solid gallium clusters: too small to melt. *Phys. Rev. Lett.* 91:215508
46. Breaux GA, Hillman DA, Neal CM, Benirschke RC, Jarrold MF. 2004. Gallium cluster "magic melters." *J. Am. Chem. Soc.* 126:8628–29
47. Breaux GA, Cao B, Jarrold MF. 2005. Second order phase transitions in amorphous gallium clusters. *J. Phys. Chem. B* 109:16575–78
48. Breaux GA, Neal CM, Cao B, Jarrold MF. 2005. Melting, pre-melting, and structural transitions in size-selected aluminum clusters with around 55 atoms. *Phys. Rev. Lett.* 94:173401
49. Neal CM, Starace AK, Jarrold MF, Joshi K, Krishnamurty S, Kanhere DG. 2007. Melting of aluminum cluster cations with 31–48 atoms: experiment and theory. *J. Phys. Chem. C* 111:17788–94
50. Neal CM, Starace AK, Jarrold MF. 2007. Melting transitions in aluminum clusters: the role of partially-melted intermediates. *Phys. Rev. B* 76:054113
51. Jarrold MF, Cao B, Starace AK, Neal CM, Judd OH. 2008. Metal clusters that freeze into high energy geometries. *J. Chem. Phys.* 129:014503
52. Starace AK, Neal CM, Cao B, Jarrold MF, Aguado A, López JM. 2008. Correlation between the latent heats and cohesive energies of metal clusters. *J. Chem. Phys.* 129:144702
53. Cao B, Starace AK, Judd OH, Jarrold MF. 2009. Phase coexistence in melting aluminum clusters. *J. Chem. Phys.* 130:204303
54. Cao B, Starace AK, Judd OH, Bhattacharyya I, Jarrold MF. 2009. Metal clusters with hidden ground states: melting and structural transitions in Al_{115}^+, Al_{116}^+, and Al_{117}^+. *J. Chem. Phys.* 131:124305
55. Starace AK, Neal CM, Cao B, Jarrold MF, Aguado A, López JM. 2009. Electronic effects on melting: comparison of aluminum cluster anions and cations. *J. Chem. Phys.* 131:044307
56. Starace AK, Cao B, Judd OH, Bhattacharyya I, Jarrold MF. 2010. Melting of size-selected aluminum nanoclusters with 84–128 atoms. *J. Chem. Phys.* 132:034302
57. Breaux GA, Benirschke RC, Jarrold MF. 2004. Melting, freezing, sublimation, and phase coexistence in sodium chloride nanocrystals. *J. Chem. Phys.* 121:6502–7
58. Neal CM, Starace AK, Jarrold MF. 2007. The melting of alloy clusters: effects of aluminum doping on gallium cluster melting. *J. Phys. Chem. A* 111:8056–61
59. Cao B, Starace AK, Neal CM, Jarrold MF, Núñez S, et al. 2008. Substituting a copper atom modifies the melting of aluminum clusters. *J. Chem. Phys.* 129:124709
60. Hock C, Strassburg S, Haberland H, von Issendorff B, Aguado A, Schmidt M. 2008. Melting-point depression by insoluble impurities: a finite size effect. *Phys. Rev. Lett.* 101:023401
61. Hock C, Schmidt M, Kuhnen R, Bartels C, Ma L, et al. 2009. Calorimetric observation of the melting of free water nanoparticles at cryogenic temperatures. *Phys. Rev. Lett.* 103:073401
62. Zhang W, Zhang F, Zhu Z. 2006. Molecular dynamics study on the melting phase transition of aluminum clusters with around 55 atoms. *Phys. Rev. B* 74:033412
63. Noya EG, Doye JPK, Calvo F. 2006. Theoretical study of the melting of aluminum clusters. *Phys. Rev. B* 73:125407
64. Li ZH, Truhlar DG. 2008. Nanosolids, slushes, and nanoliquids: characterization of nanophases in metal clusters and nanoparticles. *J. Am. Chem. Soc.* 130:12698–711

41. Reports the observation of atomic layering in liquid clusters.

42. Reports the surprising observation that small clusters can have melting temperatures that are systematically larger than the bulk material.

48. Reports the observation of premelting transitions in aluminum clusters.

55. Reports first experimental results showing the influence of electronic shells on the melting transitions of metal clusters.

65. Hsu PJ, Luo JS, Lai SK, Wax JF, Bretonnet J-L. 2008. Melting scenario in metallic clusters. *J. Chem. Phys.* 129:194302
66. Ojwang JGO, van Santen R, Kramer GJ, van Duin ACT, Goddard WA. 2008. Predictions of melting, crystallization, and local atomic arrangements of aluminum clusters using a reactive force field. *J. Chem. Phys.* 129:244506
67. Ghazi SM, Zorriasatein S, Kanhere DG. 2009. Building clusters atom-by-atom: from local order to global order. *J. Phys. Chem. A* 113:2659–62
68. Chacko S, Joshi K, Kanhere DG, Blundell SA. 2004. Why do gallium clusters have a higher melting point than the bulk? *Phys. Rev. Lett.* 92:135506
69. Joshi K, Krishnamurty S, Kanhere DG. 2006. "Magic melters" have geometrical origin. *Phys. Rev. Lett.* 96:135703
70. Krishnamurty S, Chacko S, Kanhere DG, Breaux GA, Neal CM, Jarrold MF. 2006. Size-sensitive melting characteristics of gallium clusters: comparison of experiment and theory for Ga_{17}^+ and Ga_{20}^+. *Phys. Rev. B* 73:045406
71. Joshi K, Kanhere DG, Blundell SA. 2003. Thermodynamics of tin clusters. *Phys. Rev. B* 67:235413
72. Bréchignac C, Cahuzac Ph, Leygnier J, Weiner J. 1989. Dynamics of unimolecular dissociation of sodium cluster ions. *J. Chem. Phys.* 90:1492–98
73. Neal CM, Starace AK, Jarrold MF. 2007. Ion calorimetry: using mass spectrometry to measure melting points. *J. Am. Soc. Mass Spectrom.* 18:74–81
74. Jarrold MF, Honea EC. 1991. Dissociation of large silicon clusters: the approach to bulk behavior. *J. Phys. Chem.* 95:9181–85
75. Jarrold MF. 1995. Drift-tube studies of atomic clusters. *J. Phys. Chem.* 99:11–21
76. Johnston RL. 2003. Evolving better nanoparticles: genetic algorithms for optimising cluster geometries. *Dalton Trans.* 22:4193–207
77. Wales DJ, Doye JPK. 1997. Global optimization by basin-hopping and the lowest energy structures of Lennard-Jones clusters containing up to 110 atoms. *J. Phys. Chem. A* 101:5111–16
78. Calvo F. 2009. Non-genetic global optimization methods in molecular science: an overview. *Comput. Mater. Sci.* 45:8–15
79. Allen MP, Tildesley DJ. 1987. *Computer Simulation of Liquids*. New York: Oxford Univ. Press
80. Calvo F, Wales DJ. 2008. Relaxation of caloric curves on complex potential energy surfaces. *J. Chem. Phys.* 128:154501
81. Calvo F, Labastie P. 2005. Numerical simulations of the shape and "phase transitions" in finite systems. *Eur. J. Phys.* 26:S23–30
82. Calvo F. 2005. All-exchanges parallel tempering. *J. Chem. Phys.* 123:124106
83. Voth GA. 1996. Path-integral centroid methods in quantum statistical mechanics and dynamics. *Adv. Chem. Phys.* 93:135–218
84. Bonacić-Koutecký V, Fantucci P, Koutecký J. 1991. Quantum chemistry of small clusters of elements of groups IA, IB, and IIA: fundamental concepts, predictions, and interpretation of experiments. *Chem. Rev.* 91:1035–108
85. Dreizler R, Gross E. 1995. *Density Functional Theory*. New York: Plenum
86. Payne MC, Teter MP, Allan DC, Arias TA, Joannopoulos JD. 1992. Iterative minimization techniques for ab initio total energy calculations: molecular dynamics and conjugate gradients. *Rev. Mod. Phys.* 64:1045–97
87. Finnis M. 2003. *Interatomic Forces in Condensed Matter*. New York: Oxford Univ. Press
88. Ho GS, Huang C, Carter EA. 2007. Describing metal surfaces and nanostructures with orbital-free density functional theory. *Curr. Opin. Solid State Mater. Sci.* 11:57–61
89. Delfour L, Creuze J, Legrand B. 2009. Exotic behavior of the outer shell of bimetallic nanoalloys. *Phys. Rev. Lett.* 103:205701
90. Calvo F, Cottancin E, Broyer M. 2008. Segregation, core alloying, and shape transitions in bimetallic nanoclusters: Monte Carlo simulations. *Phys. Rev. B* 77:121406
91. De Heer WA. 1993. The physics of simple metal clusters: experimental aspects and simple models. *Rev. Mod. Phys.* 65:611–76

73. Describes the multicollision-induced dissociation method used to measure the heat capacities of aluminum clusters.

92. Röthlisberger U, Andreoni W. 1991. Structural and electronic properties of sodium microclusters (n = 2–20) at low and high temperatures: new insights from ab initio molecular dynamics studies. *J. Chem. Phys.* 94:8129–51
93. Poteau R, Spiegelmann F, Labastie P. 1994. Isomerizations and phase transitions in small sodium clusters. *Z. Phys. D* 30:57–68
94. Blaise P, Blundell SA, Guet C. 1997. Extended Thomas-Fermi molecular dynamics of sodium clusters. *Phys. Rev. B* 55:15856–67
95. Aguado A, López JM, Alonso JA, Stott MJ. 1999. Orbital-free molecular dynamics simulations of melting in Na_8 and Na_{20}: melting in steps. *J. Chem. Phys.* 111:6026–35
96. Calvo F, Spiegelmann F. 1999. Geometric size effects in the melting of sodium clusters. *Phys. Rev. Lett.* 82:2270–73
97. Calvo F, Spiegelmann F. 2000. Mechanisms of phase transitions in sodium clusters: from molecular to bulk behavior. *J. Chem. Phys.* 112:2888–908
98. Vichare A, Kanhere DG, Blundell SA. 2001. Model dependence of the thermodynamic properties of Na_8 and Na_{20} clusters studied with ab initio electronic structure methods. *Phys. Rev. B* 64:045408
99. Aguado A, López JM, Alonso JA, Stott MJ. 2001. Melting in large sodium clusters: an orbital-free molecular dynamics study. *J. Phys. Chem. B* 105:2386–92
100. Manninen K, Rytkönen A, Manninen M. 2004. Influence of electronic and geometric properties on melting of sodium clusters. *Eur. Phys. J. D* 29:39–47
101. Calvo F, Spiegelmann F. 2004. On the premelting features in sodium clusters. *J. Chem. Phys.* 120:9684–89
102. Rytkönen A, Häkkinen H, Manninen M. 1998. Melting and octupole deformation of Na_{40}. *Phys. Rev. Lett.* 80:3940–43
103. Rytkönen A, Häkkinen H, Manninen M. 1999. Melting and multipole deformation of sodium clusters. *Eur. Phys. J. D* 9:451–54
104. Manninen K, Häkkinen H, Manninen M. 2004. Electronic structure and thermal behavior of a magic Na_{59}^+ cluster. *Phys. Rev. A* 70:023203
105. Manninen K, Häkkinen H, Manninen M. 2006. Ab initio simulations of $Na_{59}^+$and Na_{93}^+. *Comput. Mater. Sci.* 35:158–62
106. Chacko S, Kanhere DG, Blundell SA. 2005. First-principles calculations of melting temperatures for free Na clusters. *Phys. Rev. B* 71:155407

107. OF-DFT molecular dynamics simulations that reproduce the size dependency of the melting temperatures for sodium clusters.

107. Aguado A, López JM. 2005. Anomalous size dependence of the melting temperatures of free sodium clusters: an explanation for the calorimetry experiments. *Phys. Rev. Lett.* 94:233401

108. Noya EG, Doye JPK, Wales DJ, Aguado A. 2007. Geometric magic numbers of sodium clusters: interpretation of the melting behaviour. *Eur. Phys. J. D* 43:57–60
109. Kostko O, Huber B, Moseler M, von Issendorff B. 2007. Structure determination of medium-sized sodium clusters. *Phys. Rev. Lett.* 98:043401
110. Aguado A. 2005. Competing thermal activation mechanisms in the melting-like transition of Na_n (n = 135–147) clusters. *J. Phys. Chem. B* 109:13043–48
111. Ghazi SM, Lee MS, Kanhere DG. 2008. The effects of electronic structure and charge state on thermodynamic properties: an ab initio molecular dynamics investigation on neutral and charged clusters of Na_{39}, Na_{40} and Na_{41}. *J. Chem. Phys.* 128:104701
112. Lee MS, Kanhere DG. 2007. Effects of geometric and electronic structure on the finite temperature behavior of Na_{58}, Na_{57} and Na_{55} clusters. *Phys. Rev. B* 75:125427
113. Ellert C, Schmidt M, Schmitt C, Reiners T, Haberland H. 1995. Temperature dependence of the optical response of small, open shell sodium clusters. *Phys. Rev. Lett.* 75:1731–34
114. Schmidt M, Ellert C, Kronmüller W, Haberland H. 1999. Temperature dependence of the optical response of sodium cluster ions Na_n^+, with $4 \leq n \leq 16$. *Phys. Rev. B* 59:10970–79
115. Lee MS, Chacko S, Kanhere DG. 2005. First-principles investigation of finite-temperature behavior in small sodium clusters. *J. Chem. Phys.* 123:164310
116. Zorriasatein S, Lee MS, Kanhere DG. 2007. Electronic structure, equilibrium geometries, and finite-temperature properties of Na_n (n = 39–55) from first principles. *Phys. Rev. B* 76:165414
117. Aguado A, López JM. 2006. Small sodium clusters that melt gradually: melting mechanisms in Na_{30}. *Phys. Rev. B* 74:115403

118. Aguado A, Molina LM, López JM, Alonso JA. 2001. Melting behaviour of large disordered sodium clusters. *Eur. Phys. J. D* 15:221–27
119. Núñez S, López JM, Aguado A. 2009. Atomic layering and related postmelting effects in small liquid metal clusters. *Phys. Rev. B* 79:165429
120. Wales DJ. 2003. *Energy Landscapes with Applications to Clusters, Biomolecules and Glasses*. Cambridge, UK: Cambridge Univ. Press
121. Reyes-Nava JA, Garzón IL, Michaelian K. 2003. Negative heat capacity of sodium clusters. *Phys. Rev. B* 67:165401
122. Calvo F, Wales DJ, Doye JPK, Berry RS, Labastie P, Schmidt M. 2008. Comment on "Critical analysis of negative heat capacity in nanoclusters." *Eur. Phys. Lett.* 82:43003; Reply. *Eur. Phys. Lett.* 82:43004
123. Michaelian K, Santamaría-Holek I. 2007. Critical analysis of negative heat capacity in nanoclusters. *Eur. Phys. Lett.* 79:40005
124. Lynden-Bell D, Lynden-Bell RM. 2008. Negative heat capacities do occur. Comment on "Critical analysis of negative heat capacity in nanoclusters." *Eur. Phys. Lett.* 82:43001; Reply. *Eur. Phys. Lett.* 82:43002
125. Poland D. 2007. Intermediates in the melting transitions of aluminum nanoclusters. *J. Chem. Phys.* 126:054507
126. Nauchitel VV, Pertsin AJ. 1980. A Monte Carlo study of the structure and thermodynamic behavior of small Lennard-Jones clusters. *Mol. Phys.* 40:1341–55
127. Cheng H-P, Berry RS. 1992. Surface melting of clusters and implication for bulk matter. *Phys. Rev. A* 45:7969–80
128. Lee YJ, Lee E-K, Kim S, Nieminen RM. 2001. Effect of potential energy distribution on the melting of clusters. *Phys. Rev. Lett.* 86:999–1002
129. Ghazali A, Lévy J-CS. 1997. Structural transitions in clusters. *Phys. Lett A* 228:291–96
130. Cleveland CL, Luedtke WD, Landman U. 1998. Melting of gold clusters: icosahedral precursors. *Phys. Rev. Lett.* 81:2036–39
131. Pundt A, Dornheim M, Guerdane M, Teichlet H, Ehrenberg H, et al. 2002. Evidence for a cubic-to-icosahedral transition of quasi-free Pd-H-clusters controlled by the hydrogen content. *Eur. Phys. J. D* 19:333–37
132. Li TX, Lee SM, Han SJ, Wang GH. 2002. Structural transitions in Au_{55} isomers. *Phys. Lett. A* 300:86–92
133. Schebarchov D, Hendy SC. 2005. Transition from icosahedral to decahedral structure in a coexisting solid-liquid nickel cluster. *Phys. Rev. Lett.* 95:116101
134. Kuo C-L, Clancy P. 2005. Melting and freezing characteristics and structural properties of supported and unsupported gold nanoclusters. *J. Phys. Chem. B* 109:13743–54
135. Zhang Z, Hu W, Xiao S. 2006. Melting, melting competition, and structural transitions between shell-closed icosahedral and octahedral nickel nanoclusters. *Phys. Rev. B* 73:125443
136. Schebarchov D, Hendy SC. 2006. Solid-liquid phase coexistence and structural transitions in palladium clusters. *Phys. Rev. B* 73:121402
137. Doye JPK, Wales DJ. 1998. Thermodynamics of global optimization. *Phys. Rev. Lett.* 80:1357–60
138. Doye JPK, Calvo F. 2002. Entropic effects on the structure of Lennard-Jones clusters. *J. Chem. Phys.* 116:8307–17
139. Mandelshtam VA, Frantsuzov PA, Calvo F. 2006. Structural transitions and melting in LJ_{74-78} Lennard-Jones clusters from adaptive exchange Monte Carlo simulations. *J. Phys. Chem. A* 110:5326–32
140. Noya EG, Doye JPK. 2006. Structural transitions in the 309-atom magic number Lennard-Jones cluster. *J. Chem. Phys.* 124:104503
141. Mandelshtam VA, Frantsuzov PA. 2006. Multiple structural transformations in Lennard-Jones clusters: generic versus size-specific behavior. *J. Chem. Phys.* 124:204511
142. Sharapov VA, Mandelshtam VA. 2007. Solid-solid structural transformations in Lennard-Jones clusters: accurate simulations versus the harmonic superposition approximation. *J. Phys. Chem. A* 111:10284–91
143. Zhan L, Chen JZY, Liu WK. 2007. Determination of structural transitions of atomic clusters from local and global bond orientational order parameters. *J. Chem. Phys.* 127:141101

122. Reports theoretical and computer simulation evidence for a negative microcanonical heat capacity in a sodium cluster.

144. Klots CE. 1988. Evaporation from small particles. *J. Phys. Chem.* 92:5864–68
145. Ray U, Jarrold MF, Bower JE, Kraus JS. 1989. Photodissociation kinetics of aluminum cluster ions: determination of cluster dissociation energies. *J. Chem. Phys.* 91:2912–21
146. Radi PP, Hsu MT, Brodbelt-Lustig J, Rincon M, Bowers MT. 1990. Evaporation of covalent clusters: unimolecular decay of energized size selected carbon cluster ions (C_n^+, $5 \leq n \leq 100$). *J. Chem. Phys.* 92:4817–22
147. Hales DA, Lian L, Armentrout PB. 1990. Collision-induced dissociation of Nb_n^+ ($n = 2$–11): bond energies and dissociation pathways. *Int. J. Mass Spectrom. Ion Proc.* 102:269–301
148. Cao B, Starace AK, Judd OH, Jarrold MF. 2009. Melting dramatically enhances the reactivity of aluminum nanoclusters. *J. Am. Chem. Soc.* 131:2446–47
149. Cao B, Starace AK, Judd OH, Bhattacharyya I, Jarrold MF, et al. 2010. Activation of dinitrogen by solid and liquid aluminum nanoclusters: a combined experimental and theoretical study. *J. Am. Chem. Soc.* 132:12906–18

Annual Review of
Physical Chemistry
Volume 62, 2011

Contents

Indexes

Errata

An online log of corrections to *Annual Review of Physical Chemistry* articles may be found at http://physchem.annualreviews.org/errata.shtml